# Finite Temperature Large $N$ Gauge Theory with Quarks in an External Magnetic Field

**Tameem Albash, Veselin Filev, Clifford V. Johnson, Arnab Kundu**

*Department of Physics and Astronomy*
*University of Southern California*
*Los Angeles, CA 90089-0484, U.S.A.*

talbash, filev, johnson1, akundu [at] usc.edu

**Abstract**

Using a ten dimensional dual string background, we study aspects of the physics of finite temperature large $N$ four dimensional $SU(N)$ gauge theory, focusing on the dynamics of fundamental quarks in the presence of a background magnetic field. At vanishing temperature and magnetic field, the theory has $\mathcal{N} = 2$ supersymmetry, and the quarks are in hypermultiplet representations. In a previous study, similar techniques were used to show that the quark dynamics exhibit spontaneous chiral symmetry breaking. In the present work we begin by establishing the non–trivial phase structure that results from finite temperature. We observe, for example, that above the critical value of the field that generates a chiral condensate spontaneously, the meson melting transition disappears, leaving only a discrete spectrum of mesons at any temperature. We also compute several thermodynamic properties of the plasma.

# 1 Introduction

In recent years, the understanding of the dynamics of a variety of finite temperature gauge theories at strong coupling has been much improved by employing several techniques from string theory to capture the physics. The framework is that of holographic [1] gauge/gravity duality, in which the physics of a non–trivial ten dimensional string theory background can be precisely translated into that of the gauge theory for which the rank ($N$) of the gauge group is large[2, 3, 4, 5], while the number ($N_f$) of fundamental flavours of quark is small compared to $N$ (see ref.[6]). Many aspects of the gauge theory, at strong 't Hooft coupling $\lambda = g^2_{\rm YM}N$, become accessible to computation since the string theory background is in a regime where the necessary string theory computations are classical or semi–classical, with geometries that are weakly curved[2] (characteristic radii in the geometry are set by $\lambda$).

These studies are not only of considerable interest in their own right, but have potential phenomenological applications, since there are reasons to suspect that they are of relevance to the dynamics of quark matter in extreme environments such as heavy ion collision experiments, where the relevant phase seems to be a quark–gluon plasma. While the string theory duals of QCD are not known, and will be certainly difficult to obtain computational control over (the size $N$ of the gauge group there is small, and the number, $N_f$, of quark flavours is comparable to $N$) it is expected (and a large and growing literature of evidence seems to support this – see below) that there are certain features of the physics from these accessible models that may persist to the case of QCD, at least when in a strongly coupled plasma phase. Well–studied examples have included various hydrodynamic properties, such as the ratio of shear viscosity to entropy, as well as important phenomenological properties of the interactions between quarks and quark jets with the plasma. Results from these sorts of computations in the string dual language have compared remarkably well with QCD phenomenological results from the heavy ion collision experiments at RHIC (see e.g., refs. [9, 10, 11, 12, 13, 14]), and have proven to be consistent with and supplementary to results from the lattice gauge theory approach.

There are many other phenomena of interest to study in a controllable setting, such as confinement, deconfinement (and the transition between them), the spectrum and dynamics of baryons and mesons, and spontaneous chiral symmetry breaking. These models provide a remarkably clear theoretical laboratory for such physics, as shown for example in some of the early work[7, 8] making use of the understanding of the introduction of fundamental quarks. Some of the results of these types of studies are also likely to be of interest for studies of QCD, while others will help map out the possibilities of what types of physics are available

in gauge theories in general, and guide us toward better control of the QCD physics that we may be able to probe using gauge/string duals.

This is the spirit of our current paper[1]. Here, we uncover many new results for a certain gauge theory at finite temperature and in the presence of a background external magnetic field, building on work done recently[15, 25] on the same theory at zero temperature.

At vanishing temperature and magnetic field, the large $N$ $SU(N)$ gauge theory has $\mathcal{N}=2$ supersymmetry, and the quarks are in hypermultiplet representations. Nevertheless, just as for studies of the even more artificial $\mathcal{N}=4$ pure gauge theory, the physics at finite temperature — that of a strongly interacting plasma of quarks and gluons in a variety of phases — has a lot to teach us about gauge theory in general, and possibly QCD in particular.

In section two we describe the holographically dual ten–dimensional geometry and the embedding of the probe D7–brane into it. In section three we extract the physics of the probe dynamics, using both analytic and numerical techniques. It is there that we deduce the phase diagram. In section four we present our computations of various thermodynamic properties of the system in various phases, and in sections five and six we present our computations and results for the low–lying parts of the spectra of various types of mesons in the theory. We conclude with a brief discussion in section seven.

# 2 The String Background

Consider the $AdS_5$–Schwarzschild$\times S^5$ solution given by:

$$\begin{aligned} ds^2/\alpha' &= -\frac{u^4-b^4}{R^2u^2}dt^2+\frac{u^2}{R^2}d\vec{x}^2+\frac{R^2u^2}{u^4-b^4}du^2+R^2d\Omega_5^2\ , \\ \text{where}\quad d\Omega_5^2 &= d\theta^2+\cos^2\theta d\Omega_3^2+\sin^2\theta d\phi^2\ , \\ \text{and}\quad d\Omega_3^2 &= d\psi^2+\cos^2\psi d\beta+\sin^2\theta d\gamma^2\ . \end{aligned} \tag{1}$$

The dual gauge theory will inherit the time and space coordinates $t\equiv x^0$ and $\vec{x}\equiv(x^1,x^2,x^3)$ respectively. Also, in the solution above, $u\in[0,\infty)$ is a radial coordinate on the asymptotically $AdS_5$ geometry and we are using standard polar coordinates on the $S^5$. The scale $R$ determines the gauge theory 't Hooft coupling according to $R^2=\alpha'\sqrt{g_{\rm YM}^2N}$. For the purpose of our study it will be convenient [7] to perform the following change of variables:

$$\begin{aligned} r^2 &= \frac{1}{2}(u^2+\sqrt{u^4-b^4})=\rho^2+L^2\ , \\ \text{with}\quad \rho &= r\cos\theta\ ,\ L=r\sin\theta\ . \end{aligned} \tag{2}$$

[1]We note that another group will present results in this area in a paper to appear shortly[26].

The expression for the metric now takes the form:

$$ds^2/\alpha' = -\left(\frac{(4r^4-b^4)^2}{4r^2R^2(4r^4+b^4)}\right)dt^2 + \frac{4r^4+b^4}{4R^2r^2}d\vec{x}^2 + \frac{R^2}{r^2}(d\rho^2+\rho^2 d\Omega_3^2 + dL^2 + L^2 d\phi^2) \ .$$

Following ref. [6], we introduce fundamental matter into the gauge theory by placing D7–brane probes into the dual supergravity background. The probe brane is parametrised by the coordinates $\{x_0, x_1, x_2, x_3, \rho, \psi, \beta, \gamma\}$ with the following ansatz for its embedding:

$$\phi \equiv \text{const}, \quad L \equiv L(\rho) \ .$$

In order to introduce an external magnetic field, we excite a pure gauge $B$–field along the $(x^2, x^3)$ directions [15]:

$$B = H dx^2 \wedge dx^3, \tag{3}$$

where $H$ is a real constant. As explained in ref. [15], while this does not change the supergravity background, it has a non–trivial effect on the physics of the probe, which is our focus. To study the effects on the probe, let us consider the general (Abelian) DBI action:

$$S_{DBI} = -N_f T_{D7} \int_{\mathcal{M}_8} d^8\xi \ \det{}^{1/2}(P[G_{ab}+B_{ab}] + 2\pi\alpha' F_{ab}) \ , \tag{4}$$

where $T_{D7} = \mu_7/g_s = [(2\pi)^7\alpha'^4 g_s]^{-1}$ is the D7–brane tension, $P[G_{ab}]$ and $P[B_{ab}]$ are the induced metric and induced $B$–field on the D7–branes' world–volume, $F_{ab}$ is the world–volume gauge field, and $N_f = 1$ here. It was shown in ref. [15] that, for the $\mathrm{AdS}_5 \times S^5$ geometry, we can consistently set the gauge field $F_{ab}$ to zero to leading order in $\alpha'$, and the same argument applies to the finite temperature case considered here. The resulting Lagrangian is:

$$\mathcal{L} = -\rho^3\left(1 - \frac{b^8}{16\left(\rho^2+L(\rho)^2\right)^4}\right)\left\{1 + \frac{16H^2\left(\rho^2+L(\rho)^2\right)^2 R^4}{\left(b^4+4\left(\rho^2+L(\rho)^2\right)^2\right)^2}\right\}^{\frac{1}{2}}\sqrt{1+L'(\rho)^2} \ . \tag{5}$$

For large $\rho \gg b$, the Lagrangian asymptotes to:

$$\mathcal{L} \approx -\rho^3\sqrt{1+L'(\rho)^2} \ , \tag{6}$$

which suggests the following asymptotic behavior for the embedding function $L(\rho)$:

$$L(\rho) = m + \frac{c}{\rho^2} + \dots \ , \tag{7}$$

where the parameters $m$ (the asymptotic separation of the D7 and D3–branes) and $c$ (the degree of transverse bending of the D7–brane in the $(\rho, \phi)$ plane) are related to the bare quark mass $m_q = m/2\pi\alpha'$ and the fermionic condensate $\langle\bar{\psi}\psi\rangle \propto -c$ respectively [8] (this calculation is repeated in appendix A). It was shown in ref. [15] that the presence of the external magnetic field spontaneously breaks the chiral symmetry of the dual gauge theory (it generates a non–zero $\langle\bar{\psi}\psi\rangle$ at zero $m$). However[7], the effect of the finite temperature is to melt the mesons and restore the chiral symmetry at zero bare quark mass. Therefore, we have two competing processes depending on the magnitudes of the magnetic field $H$ and the temperature $T = b/\pi R^2$. This suggests an interesting two dimensional phase diagram for the system, which we shall study in detail later.

To proceed, it is convenient to define the following dimensionless parameters:

$$\begin{aligned} \tilde{\rho} &= \frac{\rho}{b}\,, \quad \eta = \frac{R^2}{b^2}H\,, \quad \tilde{m} = \frac{m}{b}\,, \\ \tilde{L}(\tilde{\rho}) &= \frac{L(b\tilde{\rho})}{b} = \tilde{m} + \frac{\tilde{c}}{\tilde{\rho}^2} + \dots\,. \end{aligned} \tag{8}$$

This leads to the Lagrangian:

$$\tilde{\mathcal{L}} = -\tilde{\rho}^3 \left(1 - \frac{1}{16\left(\tilde{\rho}^2 + \tilde{L}(\tilde{\rho})^2\right)^4}\right) \left\{1 + \frac{16\left(\tilde{\rho}^2 + \tilde{L}(\tilde{\rho})^2\right)^2 \eta^2}{\left(1 + 4\left(\tilde{\rho}^2 + \tilde{L}(\tilde{\rho})^2\right)^2\right)^2}\right\}^{\frac{1}{2}} \sqrt{1 + \tilde{L}'(\tilde{\rho})^2}\,. \tag{9}$$

For small values of $\eta$, the analysis of the second order, non–linear differential equation for $\tilde{L}(\tilde{\rho})$ derived from equation (9) follows closely that performed in refs. [7, 16, 17]. The solutions split into two classes: the first class are solutions corresponding to embeddings that wrap a shrinking $S^3$ in the $S^5$ part of the geometry and (when the $S^3$ vanishes) closes at some finite radial distance $r$ above the black hole's horizon, which is located at $r = b/\sqrt{2}$. These embeddings are referred to as 'Minkowski' embeddings. The second class of solutions correspond to embeddings falling into the black hole, since the $S^1$ of the Euclidean section, on which the D7–branes are wrapped, shrinks away there. These embeddings are referred to as 'black hole' embeddings. There is also a critical embedding separating the two classes of solutions which has a conical singularity at the horizon, where the $S^3$ wrapped by the D7–brane shrinks to zero size, along with the $S^1$. If one calculates the free energy of the embeddings, one can show [7, 16, 17] that it is a multi–valued function of the asymptotic separation $m$, which amounts to a first order phase transition of the system (giving a jump in the condensate) for some critical bare quark mass $m_{\rm cr}$. (For fixed mass, we may instead

consider this to be a critical temperature.) We show in this paper that the effect of the magnetic field is to decrease this critical mass, and, at some critical magnitude of the parameter $\eta_{\rm cr}$, the critical mass drops to zero. For $\eta > \eta_{\rm cr}$ the phase transition disappears, and only the Minkowski embeddings are stable states in the dual gauge theory, possessing a discrete spectrum of states corresponding to quarks and anti–quarks bound into mesons. Furthermore, at zero bare quark mass, we have a non–zero condensate and the chiral symmetry is spontaneously broken.

# 3 Properties of the Solution

## 3.1 Exact Results at Large Mass

It is instructive to first study the properties of the solution for $\tilde{m} \gg 1$. This approximation holds for finite temperature, weak magnetic field, and large bare quark mass $m$, or, equivalently, finite bare quark mass $m$, low temperature, and weak magnetic field.

In order to analyze the case $\tilde{m} \gg 1$, let us write $\tilde{L}(\tilde{\rho}) = \tilde{a} + \zeta(\tilde{\rho})$ for $\tilde{a} \gg 1$ and linearize the equation of motion derived from equation (9), while leaving only the first two leading terms in $(\rho^2 + \tilde{m}^2)^{-1}$. The result is:

$$\partial_{\tilde{\rho}}(\tilde{\rho}^3\zeta') - \frac{2\eta^2}{(\tilde{m}^2+\tilde{\rho}^2)^3}\tilde{m} + \frac{2(\eta^2+1)^2-1}{2(\tilde{m}^2+\tilde{\rho}^2)^5}\tilde{m} + O(\zeta) = 0 \ . \tag{10}$$

Ignoring the $O(\zeta)$ terms in equation (10), the general solution takes the form:

$$\zeta(\tilde{\rho}) = -\frac{\eta^2}{4\rho^2(\tilde{m}^2+\tilde{\rho}^2)}\tilde{m} + \frac{2(\eta^2+1)^2-1}{96\tilde{\rho}^2(\tilde{m}^2+\tilde{\rho}^2)^3}\tilde{m} \ , \tag{11}$$

where we have taken $\zeta'(0) = \zeta(0) = 0$. By studying the asymptotic behavior of this solution, we can extract the following:

$$\begin{aligned} \tilde{m} &= \tilde{a} - \frac{\eta^2}{4\tilde{a}^3} + \frac{1+4\eta^2+2\eta^4}{32\tilde{a}^7} + O\left(\frac{1}{\tilde{a}^7}\right) \ , \\ \tilde{c} &= \frac{\eta^2}{4\tilde{a}} - \frac{1+4\eta^2+2\eta^4}{96\tilde{a}^5} + O\left(\frac{1}{\tilde{a}^7}\right) \ . \end{aligned} \tag{12}$$

By inverting the expression for $\tilde{m}$, we can express $\tilde{c}$ in terms of $\tilde{m}$:

$$\tilde{c} = \frac{\eta^2}{4\tilde{m}} - \frac{1+4\eta^2+8\eta^4}{96\tilde{m}^5} + O\left(\frac{1}{\tilde{m}^7}\right) \ . \tag{13}$$

Finally, after going back to dimensionful parameters, we can see that the theory has developed a fermionic condensate:

$$\langle\bar{\psi}\psi\rangle \propto -c = -\frac{R^4}{4m}H^2 + \frac{b^8 + 4b^4R^4H^2 + 8R^8H^4}{96m^5} \ . \tag{14}$$

The results of the above analysis can be trusted only for finite bare quark mass and sufficiently low temperature and weak magnetic field. As can be expected, the physically interesting properties of the system should be described by the full non–linear equation of motion of the D7–brane. To explore these we need to use numerical techniques.

## 3.2 Numerical Analysis

We solve the differential equation derived from equation (9) numerically using Mathematica. It is convenient to use infrared initial conditions [17, 18]. For the Minkowski embeddings, based on symmetry arguments, the appropriate initial conditions are:

$$\tilde{L}(\tilde{\rho})|_{\tilde{\rho}=0} = L_{\rm in}, \quad \tilde{L}'(\tilde{\rho})|_{\tilde{\rho}=0} = 0 \ . \tag{15}$$

For the black hole embeddings, the following initial conditions:

$$\tilde{L}(\tilde{\rho})|_{\rm e.h.} = \tilde{L}_{\rm in}, \quad \tilde{L}'(\tilde{\rho})|_{\rm e.h.} = \left.\frac{\tilde{L}}{\tilde{\rho}}\right|_{\rm e.h.} \ , \tag{16}$$

ensure regularity of the solution at the event horizon. After solving numerically for $\tilde{L}(\tilde{\rho})$ for fixed value of the parameter $\eta$, we expand the solution at some numerically large $\tilde{\rho}_{\rm max}$, and, using equation (7), we generate the plot of $-\tilde{c}$ vs $\tilde{m}$. It is instructive to begin our analysis by revisiting the case with no magnetic field ($\eta = 0$), familiar from refs.[7, 16, 17]. The corresponding plot for this case is presented in figure 1. Also in the figure is a plot of the large mass analytic result of equation (13), shown as the thin black curve in the figure, descending sharply downwards from above; it can be seen that it is indeed a good approximation for $\tilde{m} > \tilde{m}_{\rm cr}$. Before we proceed with the more general case of non–zero magnetic field, we review the techniques employed in ref. [17] to determine the critical value of $\tilde{m}$. In figure 2, we have presented the region of the phase transition considerably magnified. Near the critical value $\tilde{m}_{\rm cr}$, the condensate $\tilde{c}$ is a multi-valued function of $\tilde{m}$, and we have three competing phases. The parameter $\tilde{c}$ is known[8] to be proportional to the first derivative of the free energy of the D7–brane, and therefore the area below the curve of the $-\tilde{c}$ vs $\tilde{m}$ plot is proportional to the free energy of the brane. Thus, the phase transition happens where the two shaded regions in figure 2 have equal areas; furthermore, for $\tilde{m} < \tilde{m}_{\rm cr}$, the upper–most branch of the

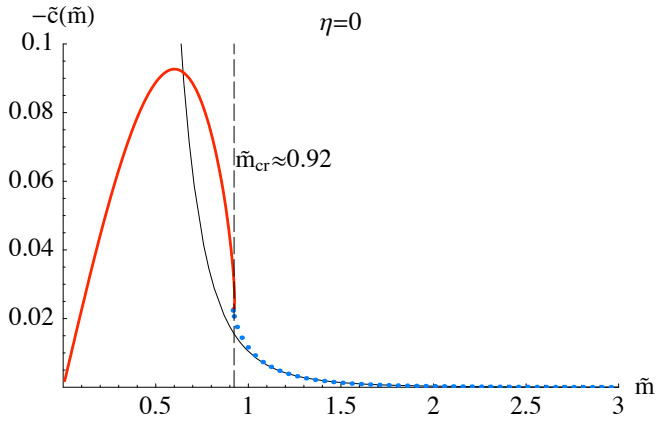


Figure 1: The solid curve starting far left (red) represents solutions falling into the black hole, the dotted (blue) curve represents solutions with shrinking $S^3$. The vertical dashed line corresponds to the critical value of $\tilde{m}$ at which the first order phase transition takes place. The solid black curve dropping sharply from above is the function derived in equation (13), corresponding to the large mass limit.

curve corresponds to the stable phase, and the lower–most branch of the curve corresponds to a meta–stable phase. For $\tilde{m} > \tilde{m}_{\rm cr}$, the lower–most branch of the curve corresponds to the stable phase, and the upper–most branch of the curve corresponds to a metastable phase. At $m = m_{\rm cr}$ we have a first order phase transition. It should be noted that the intermediate branch of the curve corresponds to an unstable phase.

Now, let us turn on a weak magnetic field. As one can see from figure 3, the effect of the magnetic field is to decrease the magnitude of $\tilde{m}_{\rm cr}$. In addition, the condensate now becomes negative for sufficiently large $\tilde{m}$ and approaches zero from below as $\tilde{m} \to \infty$. It is also interesting that equation (13) is still a good approximation for $\tilde{m} > \tilde{m}_{\rm cr}$. For sufficiently strong magnetic field, the condensate has only negative values and the critical value of $\tilde{m}$ continues to decrease, as is presented in figure 4. If we further increase the magnitude of the magnetic field, some states start having negative values of $\tilde{m}$, as shown in figure 5. The negative values of $\tilde{m}$ do not mean that we have negative bare quark masses; rather, it implies that the D7–brane embeddings have crossed $L = 0$ at least once. It was argued in ref. [7] that such embeddings are not consistent with a holographic gauge theory interpretation and are therefore to be considered unphysical. We will adopt this interpretation here, therefore taking as physical only the $\tilde{m} > 0$ branch of the $-\tilde{c}$ vs $\tilde{m}$ plots. However, the prescription for determining the value of $m_{\rm cr}$ continues to be valid, as long as the obtained value of $\tilde{m}_{\rm cr}$ is positive. Therefore, we will continue to use it in order to determine the value of $\eta \equiv \eta_{\rm cr}$ for which $\tilde{m}_{\rm cr} = 0$. As one can see in figure 6, the

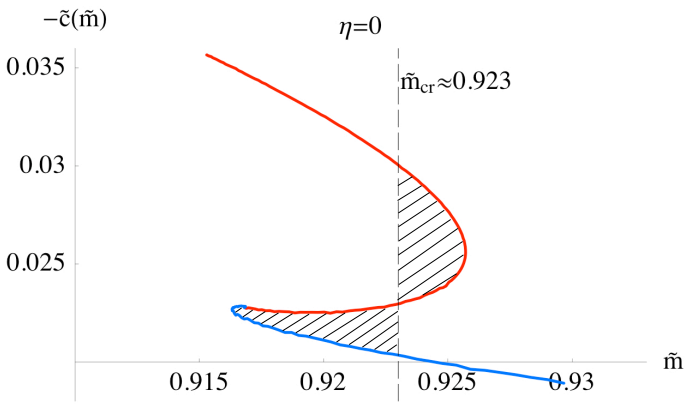


Figure 2: The area below the $(-\tilde{c}, \tilde{m})$ curve has the interpretation of the free energy of the D7–brane; thus the phase transition pattern obeys the "equal area law"— the area of the shaded regions is equal.

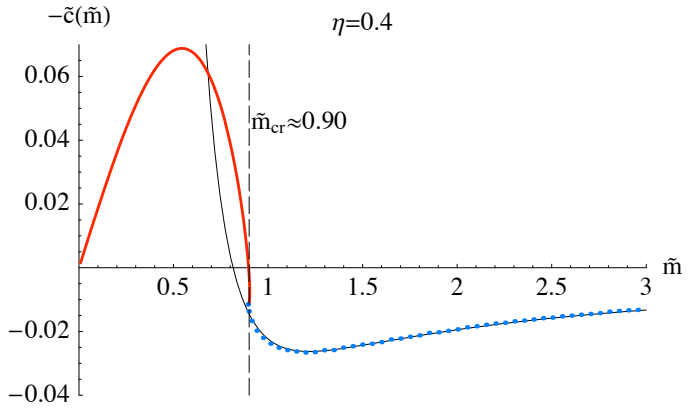


Figure 3: The effect of the weak magnetic field is to decrease the values of $\tilde{m}_{\rm cr}$ and the condensate. Equation (13) is still a good approximation for $\tilde{m} > \tilde{m}_{\rm cr}$.

value of $\eta_{\rm cr}$ that we obtain is $\eta_{\rm cr} \approx 7.89$. Note also that, for this value of $\eta$, the Minkowski $\tilde{m} = 0$ embedding has a non–zero fermionic condensate $\tilde{c}_{\rm cr}$, and hence the chiral symmetry is spontaneously broken. For $\eta > \eta_{\rm cr}$, the stable solutions are purely Minkowski embeddings, and the first order phase transition disappears; therefore, we have only one class of solutions (the blue curve) that exhibit spontaneous chiral symmetry breaking at zero bare quark mass. Some black hole embeddings remain meta–stable, but eventually all black hole embeddings become unstable for large enough $\eta$. This is confirmed by our study of the meson spectrum, which we present in later sections of the paper. The above results can be summarized in a single two dimensional phase diagram, which we present in figure 7. The curve separates the two phases corresponding to a discrete meson spectrum (light mesons) and a continuous

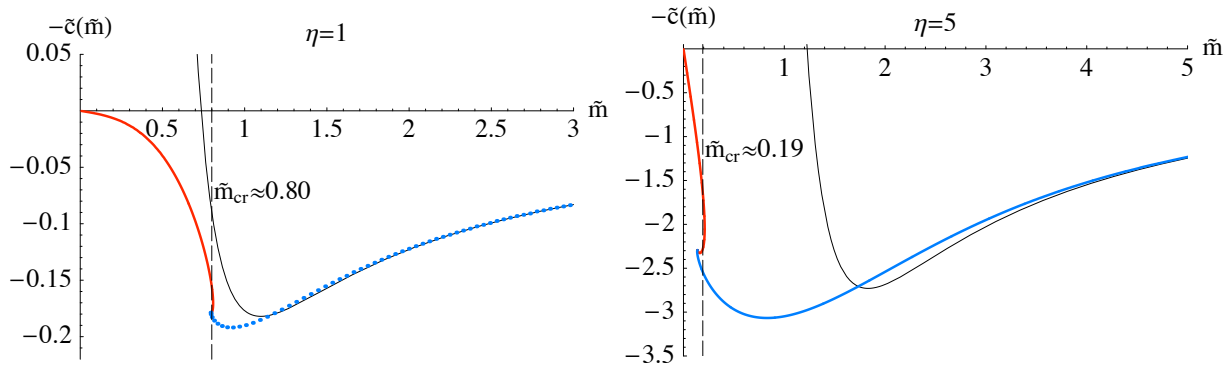


Figure 4: For strong magnetic field the condensate is negative. The value of $\tilde{m}_{\rm cr}$ continues to drop as we increase $\eta$.

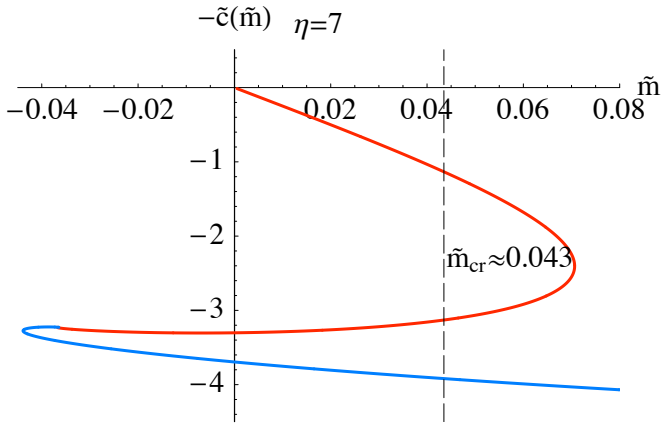


Figure 5: For sufficiently high values of $\eta$ there are states with negative $\tilde{m}$, which are considered non-physical. However the equal area law is still valid as long as $m_{\rm cr} > 0$.

meson spectrum (melted mesons) respectively. The crossing of the curve is associated with the first order phase transition corresponding to the melting of the mesons. If we cross the curve along the vertical axis, we have the phase transition described in refs. [7, 16, 17]. Crossing the curve along the horizontal axis corresponds to a transition from unbroken to spontaneously broken chiral symmetry[15], meaning the parameter $\tilde{c}$ jumps from zero to $\tilde{c}_{\rm cr} \approx 4.60$, resulting in non–zero fermionic condensate of the ground state. It is interesting to explore the dependence of the fermionic condensate at zero bare quark mass on the magnetic field. From dimensional analysis it follows that:

$$c_{\rm cr} = b^3 \tilde{c}_{\rm cr}(\eta) = \frac{\tilde{c}_{\rm cr}(\eta)}{\eta^{3/2}} R^3 H^{3/2} \ . \tag{17}$$

In the $T \to 0$ limit, we should recover the result from ref. [15]: $c_{\rm cr} \approx 0.226 R^3 H^{3/2}$, which implies that $\tilde{c}_{\rm cr}(\eta) \approx 0.226 \eta^{3/2}$ for $\eta \gg 1$. The plot of the numerically extracted dependence

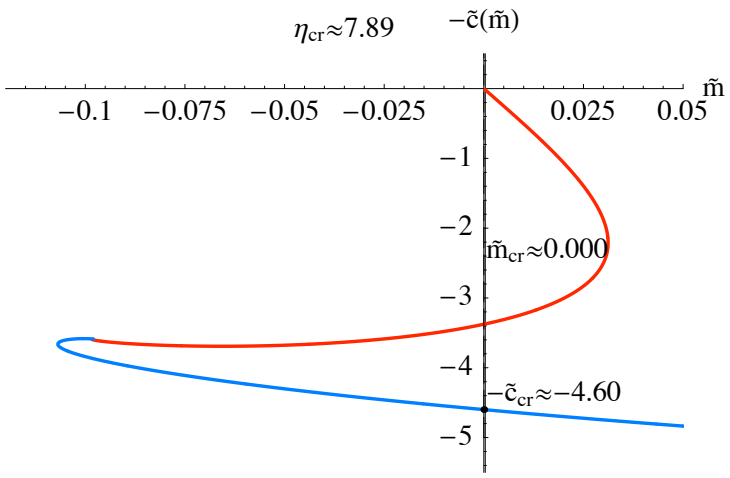


Figure 6: For $\eta = \eta_{\rm cr}$ the critical parameter $m_{\rm cr}$ vanishes. There are two $\tilde{m} = 0$ states with equal energies, one of them has non-vanishing condensate $-\tilde{c}_{\rm cr} \approx -4.60$ and therefore spontaneously breaks the chiral symmetry.

$\tilde{c}_{\rm cr}(\eta)$ is presented in figure 8; for $\eta > \eta_{\rm cr}$, $\tilde{c}_{\rm cr}(\eta)$ very fast approaches the curve $0.226\eta^{3/2}$. This suggests that the value of the chiral symmetry breaking parameter $c_{\rm cr}$ depends mainly on the magnitude of the magnetic field $H$, and only weakly on the temperature $T$.

# 4 Thermodynamics

Having understood the phase structure of the system, we now turn to the extraction of various of its important thermodynamic quantities.

## 4.1 The Free Energy

Looking at our system from a thermodynamic point of view, we must specify the potential characterizing our ensemble. We are fixing the temperature and the magnetic field, and hence the appropriate thermodynamic potential density is:

$$dF = -SdT - \mu dH \ , \tag{18}$$

where $\mu$ is the magnetization density and $S$ is the entropy density of the system. Following ref. [19], we relate the on–shell D7–brane action to the potential density $F$ via:

$$F = 2\pi^2 N_f T_{D7} I_{D7} \ , \tag{19}$$

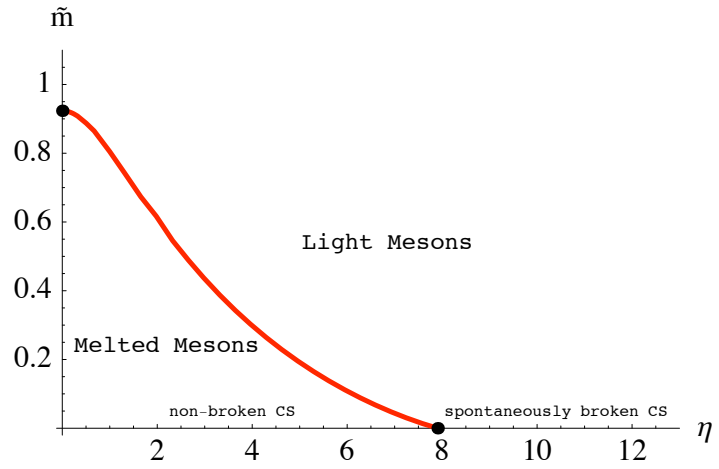


Figure 7: The curve separates the two phases corresponding to discrete meson spectrum (light mesons) and continuous meson spectrum (melted mesons).

where (here, $N_f = 1$):

$$I_{D7} = b^4 \int_{\tilde{\rho}_{\min}}^{\tilde{\rho}_{\max}} d\tilde{\rho}\tilde{\rho}^3 \left(1 - \frac{1}{16\tilde{r}^8}\right)\left(1 + \frac{16\eta^2\tilde{r}^4}{(4\tilde{r}^4+1)^2}\right)^{\frac{1}{2}} \sqrt{1+\tilde{L}'^2} + I_{\text{bound}}; \tag{20}$$

$$\eta = \frac{R^2}{b^2}H; \quad \tilde{r} = r/b; \quad \tilde{\rho} = \rho/b; \quad \tilde{L} = L/b; \quad r^2 = \rho^2 + L^2.$$

In principle, on the right hand side of equation (19), there should be terms proportional to $-H^2/2$, which subtract the energy of the magnetic field alone; however, as we comment below, the regularization of $I_{D7}$ is determined up to a boundary term of the form const $\times H^2$. Therefore, we can omit this term in the definition of $F$. The boundary action $I_{\text{bound}}$ contains counterterms designed[20] to cancel the divergent terms coming from the integral in equation (20) in the limit of $\rho_{\max} \to \infty$. A crucial observation is that the finite temperature does not introduce new divergences, and we have the usual quartic divergence from the spatial volume of the asymptotically $AdS_5$ spacetime [21]. The presence of the non–zero external magnetic field introduces a new logarithmic divergence, which can be cancelled by introducing the following counterterm:

$$-\frac{R^4}{2}\log\left(\frac{\rho_{\max}}{R}\right)\int d^4x\sqrt{-\gamma}\frac{1}{2!}B_{\mu\nu}B^{\mu\nu}\ , \tag{21}$$

where $\gamma$ is the metric of the 4–dimensional surface at $\rho = \rho_{\max}$. Note that in our case:

$$\frac{1}{2!}\sqrt{-\gamma}\,B_{\mu\nu}B^{\mu\nu} = H^2\ , \tag{22}$$

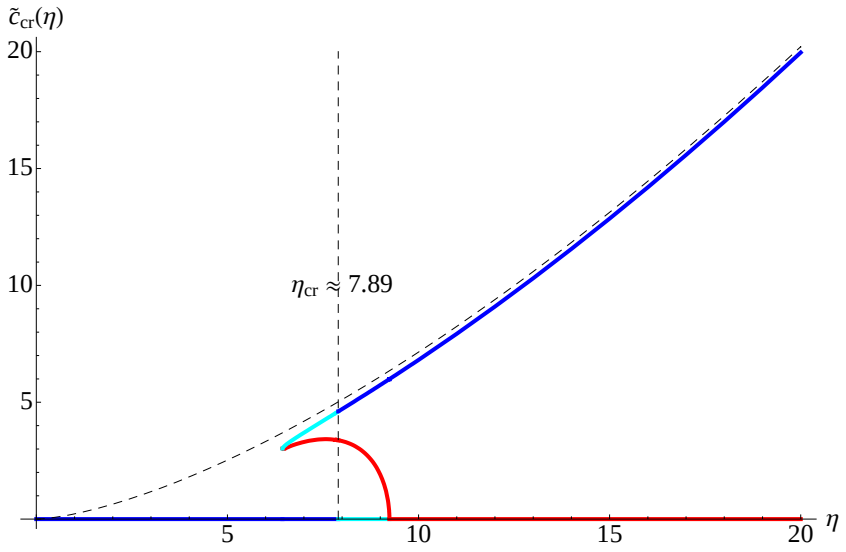


Figure 8: The solid curves are the numerically extracted dependence $\tilde{c}_{\rm cr}(\eta)$, while the dashed curve represents the expected large $\eta$ behavior $\tilde{c}_{\rm cr}(\eta) \approx 0.226\eta^{3/2}$. The solid curve segments at the bottom left and to the upper right (blue) are the stable states. The straight segment and the arc that joins it (lower right, red) and red are the unstable states. The rest (cyan) are meta–stable states.

which gives us the freedom to add finite terms of the form const $\times H^2$ at no cost to the regularized action. This makes the computation of some physical quantities scheme dependent. We will discuss this further in subsequent sections. The final form of $I_{\rm bound}$ in equation (20) is:

$$I_{\rm bound} = -\frac{1}{4}\rho_{\rm max}^4 - \frac{1}{2}R^4H^2\log\frac{\rho_{\rm max}}{R}\ . \tag{23}$$

It is instructive to evaluate the integral in equation (20) for the $L \equiv 0$ embedding at zero temperature. Going back to dimensionful coordinates we obtain:

$$\int_0^{\rho_{\rm max}} d\rho\rho^3\sqrt{1+\frac{R^4H^2}{\rho^4}} = \frac{1}{4}\rho_{\rm max}^4 + \frac{1}{2}R^4H^2\log\frac{\rho_{\rm max}}{R} + \frac{R^4H^2}{8}(1+\log 4-\log H^2) + O(\rho_{\rm max}^{-3})\ . \tag{24}$$

The first two terms are removed by the counter terms from $I_{\rm bound}$, and we are left with:

$$F(b=0,m=0,H) = 2\pi^2 N_f T_{D7}\frac{R^4H^2}{8}(1+\log 4-\log H^2)\ . \tag{25}$$

This result can be used to evaluate the magnetization density of the Yang–Mills plasma at zero temperature and zero bare quark mass. Let us proceed by writing down a more general expression for the free energy of the system. After adding the regulating terms from $I_{\rm bound}$, we obtain that our free energy is a function of $m, b, H$:

$$F(b,m,H) = 2\pi^2 N_f T_{D7} b^4 \tilde{I}_{D7}(\tilde{m},\eta^2) + F(0,0,H)\ , \tag{26}$$

where $\tilde{I}_{D7}(\tilde{m},\eta)$ is defined *via*:

$$\begin{aligned}\tilde{I}_{D7} &= \int_{\tilde{\rho}_{\rm min}}^{\tilde{\rho}_{\rm max}} d\tilde{\rho}\left(\tilde{\rho}^3\left(1-\frac{1}{16\tilde{r}^8}\right)\left(1+\frac{16\eta^2\tilde{r}^4}{(4\tilde{r}^4+1)^2}\right)^{\frac{1}{2}}\sqrt{1+\tilde{L}'^2}-\tilde{\rho}^3\right)-\tilde{\rho}_{\rm min}^4/4 \\ &\quad -\frac{1}{2}\eta^2\log\tilde{\rho}_{\rm max}-\frac{1}{8}\eta^2(1+\log 4-\log\eta^2);\quad \tilde{r}^2=\tilde{\rho}^2+\tilde{L}(\tilde{\rho})^2\ .\end{aligned} \tag{27}$$

In order to verify the consistency of our analysis with our numerical results, we derive an analytic expression for the free energy that is valid for $\tilde{m}\gg\sqrt{\eta}$. To do this we use that for large $\tilde{m}$, the condensate $\tilde{c}$ is given by equation (13), which we repeat here:

$$\tilde{c}(\tilde{m},\eta^2)=\frac{\eta^2}{4\tilde{m}}-\frac{1+4\eta^2+8\eta^4}{96\tilde{m}^5}+O(1/\tilde{m}^7)\ , \tag{28}$$

as well as the relation $\partial\tilde{I}_{D7}/\partial\tilde{m}=-2\tilde{c}$. We then have:

$$\tilde{I}_{D7}=-2\int^{\tilde{m}}\tilde{c}(\tilde{m},\eta)d\tilde{m}+\xi(\eta)=\xi(\eta)-\frac{1}{2}\eta^2\log\tilde{m}-\frac{1+4\eta^2+8\eta^4}{192\tilde{m}^4}+O(1/\tilde{m}^6)\ , \tag{29}$$

where the function $\xi(\eta)$ can be obtained by evaluating the expression for $\tilde{I}_{D7}$ from equation (27) in the approximation $\tilde{L}\approx\tilde{m}$. Note that this suggests ignoring the term $\tilde{L}'^2$, which is of order $\tilde{c}^2$. Since the leading behavior of $\tilde{c}^2$ at large $\tilde{m}$ is $1/\tilde{m}^2$, this means that the results obtained by setting $\tilde{L}'^2=0$ can be trusted to the order of $1/\tilde{m}$, and therefore we can deduce the function $\xi(\eta)$, corresponding to the zeroth order term. Another observation from earlier in this paper is that the leading behavior of the condensate is dominated by the magnetic field and therefore we can further simplify equation (27):

$$\begin{aligned}\tilde{I}_{D7} &\backsimeq \lim_{\tilde{\rho}_{\rm max}\to\infty}\int_0^{\tilde{\rho}_{\rm max}} d\tilde{\rho}\tilde{\rho}^3\left(\sqrt{1+\frac{\eta^2}{(\tilde{\rho}^2+\tilde{m}^2)^2}}-1\right)-\frac{1}{2}\eta^2\log\tilde{\rho}_{\rm max}-\frac{1}{8}\eta^2\left(1-\log\frac{\eta^2}{4}\right) \\ &= -\frac{\eta^2}{2}\log\tilde{m}-\frac{\eta^2}{8}(3-\log\frac{\eta^2}{4})+O(1/\tilde{m}^3)\ .\end{aligned} \tag{30}$$

Comparing to equation (29), we obtain:

$$\xi(\eta)=-\frac{\eta^2}{8}(3-\log\frac{\eta^2}{4})\ , \tag{31}$$

and our final expression for $\tilde{I}_{D7}$, valid for $\tilde{m}\gg\sqrt{\eta}$:

$$\tilde{I}_{D7}=-\frac{\eta^2}{8}\left(3-\log\frac{\eta^2}{4}\right)-\frac{1}{2}\eta^2\log\tilde{m}-\frac{1+4\eta^2+8\eta^4}{192\tilde{m}^4}+O(1/\tilde{m}^6)\ . \tag{32}$$

## 4.2 The Entropy

Our next goal is to calculate the entropy density of the system. Using our expressions for the free energy we can write:

$$\begin{aligned} S &= -\left(\frac{\partial F}{\partial T}\right)_H = -\pi R^2 \frac{\partial F}{\partial b} = -2\pi^3 R^2 N_f T_{D7} b^3 \left(4\tilde{I}_{D7} + b\frac{\partial \tilde{I}_{D7}}{\partial \tilde{m}}\frac{\partial \tilde{m}}{\partial b} + b\frac{\partial \tilde{I}_{D7}}{\partial \eta^2}\frac{\partial \eta^2}{\partial b}\right) \\ &= -2\pi^3 R^2 N_f T_{D7} b^3 \left(4\tilde{I}_{D7} + 2\tilde{c}\tilde{m} - 4\frac{\partial \tilde{I}_{D7}}{\partial \eta^2}\eta^2\right) = 2\pi^3 R^2 N_f T_{D7} b^3 \tilde{S}(\tilde{m}, \eta^2) \ . \end{aligned} \tag{33}$$

It is useful to calculate the entropy density at zero bare quark mass and zero fermionic condensate. To do this, we need to calculate the free energy density by evaluating the integral in equation (27) for $\tilde{L} \equiv 0$. The expression that we get for $\tilde{I}_{D7}(0, \eta^2)$ is:

$$\tilde{I}_{D7}(0, \eta^2) = \frac{1}{8}\left(1 - 2\sqrt{1+\eta^2} - \eta^2 \log\frac{(1+\sqrt{1+\eta^2})^2}{\eta^2}\right) \ . \tag{34}$$

The corresponding expression for the entropy density is:

$$S|_{m=0} = 2\pi^6 R^8 N_f T_{D7} T^3 \left(-\frac{1}{2} + \sqrt{1 + \frac{\pi^4 H^2}{R^4 T^4}}\right) \ . \tag{35}$$

One can see that the entropy density is positive and goes to zero as $T \to 0$. Our next goal is to solve for the entropy density at finite $\tilde{m}$ for fixed $\eta$. To do so, we have to integrate numerically equation (33) and generate a plot of $\tilde{S}$ versus $\tilde{m}$. However, for $\tilde{m} \gg \sqrt{\eta}$ we can derive an analytic expression for the entropy. After substituting the expression from equation (32) for $\tilde{I}_{D7}$ into equation (33) we obtain:

$$\tilde{S}(\tilde{m}, \eta^2) = \frac{1 + 2\eta^2}{24\tilde{m}^4} + \dots \ , \tag{36}$$

or if we go back to dimensionful parameters:

$$S(b, m, H) = 2\pi^3 R^2 N_f T_{D7} b^3 \left(\frac{b^4 + 2R^4 H^2}{24 m^4}\right) \ . \tag{37}$$

One can see that if we send $T \to 0$, while keeping $\eta$ fixed we get the $T^7$ behavior described in ref. [19], and therefore the (approximate; $N_f/N \ll 1$) conformal behaviour is restored in this limit. In figure 9, we present a plot of $\tilde{S}$ versus $\tilde{m}$ for $\eta = 0.4$ . The solid smooth black curve corresponds to equation (36). For this $\tilde{S}$ is positive and always a decreasing function of $\tilde{m}$. Hence, the entropy density at fixed bare quark mass $m = \tilde{m}b$, given by

$S = 2\pi^3 R^2 N_f T_{D7} m^3 \tilde{S}/\tilde{m}^3$, is also a decreasing function of $\tilde{m}$ and therefore an increasing function of the temperature, except near the phase transition (the previously described crossover from black hole to Minkowski embeddings) where an unstable phase appears that is characterized by a negative heat capacity.

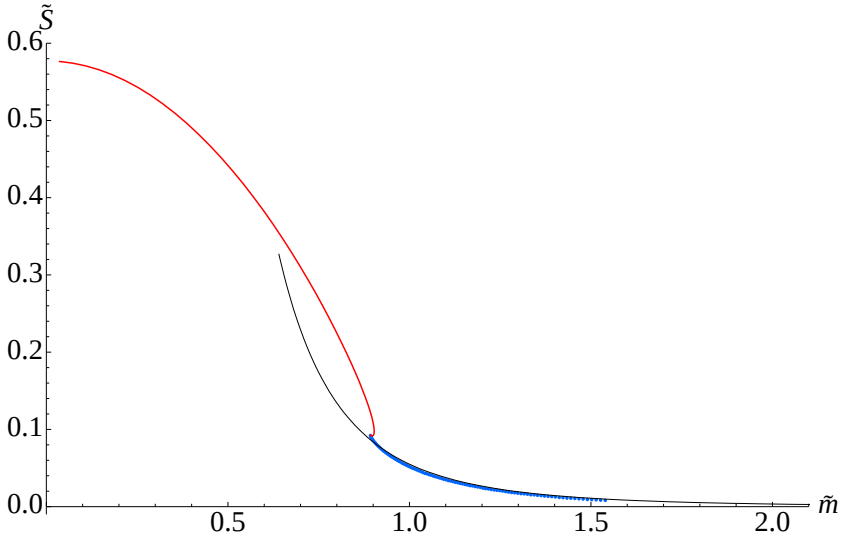


Figure 9: A plot of $\tilde{S}$ versus $\tilde{m}$ for $\eta = 0.4$ . The thin (sharply descending and extending to the right) black curve corresponds to that large mass result of equation (36).

## 4.3 The Magnetization

Let us consider equation (25) for the free energy density at zero temperature and zero bare quark mass. The corresponding magnetization density is given by:

$$\mu_0 = -\left(\frac{\partial F}{\partial H}\right)_{T,m=0} = 2\pi^2 R^4 N_f T_{D7} \frac{H}{2} \log \frac{H}{2}. \tag{38}$$

Note that this result is scheme dependent, because of the freedom to add terms of the form const $\times H^2$ to the boundary action that we discussed earlier. However, the value of the relative magnetization is given by:

$$\mu - \mu_0 = -\left(\frac{\partial F}{\partial H}\right)_T - \mu_0 = -2\pi^2 R^2 N_f T_{D7} b^2 \left(\frac{\partial \tilde{I}_{D7}}{\partial \eta}\right)_{\tilde{m}} = 2\pi^2 R^2 N_f T_{D7} b^2 \tilde{\mu} \ , \tag{39}$$

is scheme independent and is the quantity of interest in the section. In equation (39), we have defined $\tilde{\mu} = -\partial \tilde{I}_{D7}/\partial \eta|_{\tilde{m}}$ as a dimensionless parameter characterizing the relative

magnetization. Details of how the derivative is taken are discussed in appendix B. The expression for $\tilde{\mu}$ follows directly from equation (27):

$$\tilde{\mu} = \lim_{\tilde{\rho}_{\rm max}\to\infty} - \int_{\tilde{\rho}_{\rm min}}^{\tilde{\rho}_{\rm max}} d\tilde{\rho} \frac{\tilde{\rho}^3(4\tilde{r}^4-1)}{\tilde{r}^4\sqrt{(4\tilde{r}^4+1)^2+16\eta\tilde{r}^4}} + \eta\log\tilde{\rho}_{\rm max} - \frac{\eta}{2}\log\frac{\eta}{2}. \tag{40}$$

For the large $\tilde{m}$ region we use the asymptotic expression for $\tilde{I}_{D7}$ from equation (32) and obtain the following analytic result for $\tilde{\mu}$:

$$\tilde{\mu} = \frac{\eta}{2} - \frac{\eta}{2}\log\frac{\eta}{2} + \eta\log\tilde{m} + \frac{\eta(1+4\eta^2)}{24\tilde{m}^4} + O(1/\tilde{m}^6)\ . \tag{41}$$

We evaluate the above integral numerically and generate a plot of $\tilde{\mu}$ versus $\tilde{m}$. A plot of the dimensionless relative magnetization $\tilde{\mu}$ versus $\tilde{m}$ for $\eta = 0.5$ is presented in figure 10. The black curve corresponding to equation (41) shows good agreement with the asymptotic behavior at large $\tilde{m}$. It is interesting to verify the equilibrium condition $\partial\tilde{\mu}/\partial T > 0$. Note that since $\mu_0$ does not depend on the temperature, the value of this derivative is a scheme independent quantity. From equations (39) and equation (41), one can obtain:

$$\frac{\partial\mu}{\partial T} = 2\pi^3 R^4 N_f T_{D7} b\left(2\tilde{\mu} - \frac{\partial\tilde{\mu}}{\partial\tilde{m}}\tilde{m} - 2\frac{\partial\tilde{\mu}}{\partial\eta}\eta\right) = 2\pi^3 R^6 N_f T_{D7}\frac{Hb^3}{6m^4} > 0\ , \tag{42}$$

which is valid for large $m$ and weak magnetic field $H$. Note that the magnetization seems to increase with the temperature. Presumably this means that the temperature increases the "ionization" of the Yang–Mills plasma of mesons even before the phase transition occurs.

## 4.4 The Speed of Sound

It is interesting to investigate the effect of the magnetic field on the speed of sound in the Yang–Mills plasma. Following ref. [19], we use the following definition to thermodynamically determine the speed:

$$v^2 \ = \ \frac{S}{c_V} = \frac{S_{D3}+S_{D7}}{c_{V3}+c_{V7}}\ , \tag{43}$$

where $c_V$ is the density of the heat capacity at constant volume. To compute the contribution coming from the fundamental flavors in the presence of an external magnetic field, we work perturbatively in small $N_f/N_c$. First, let us recall the adjoint contribution to entropy and specific heat [19]:

$$S_{D3} \ = \ -\frac{\pi^2}{2}N^2T^3\ , \quad c_{V3} = 3S_{D3}\ . \tag{44}$$

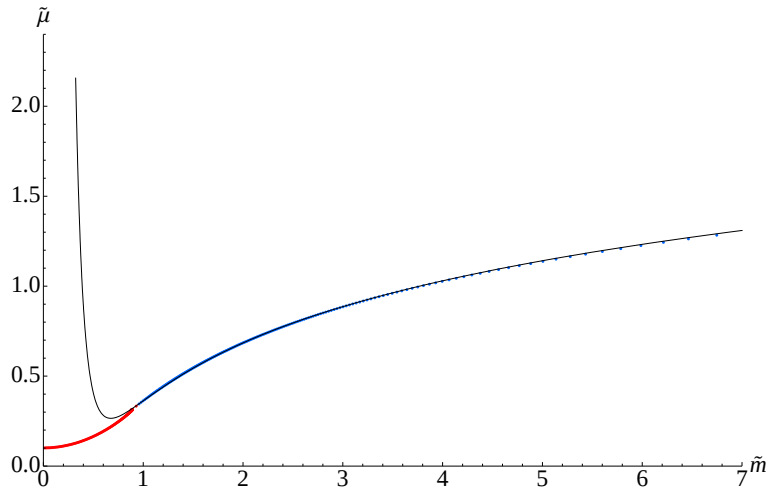


Figure 10: A plot of the dimensionless relative magnetization $\tilde{\mu}$ versus $\tilde{m}$ for $\eta = 0.5$. The thin black curve (starting with a steep descent) corresponds to the large mass result of equation (41).

To proceed, let us rewrite the entropy density of the fundamental flavours in the following form:

$$S_{D7} = -\frac{4F}{T}\left(1+\frac{2\widetilde{\mathcal{N}}\tilde{m}\tilde{c}(\pi T)^4}{4F}\right)+\frac{4}{T}\left(F_0+\widetilde{\mathcal{N}}(\pi T)^4\eta^2\frac{\partial\tilde{I}_{D7}}{\partial\eta^2}\right), \tag{45}$$

where $\widetilde{\mathcal{N}} = 2\pi^2 N_f T_{D7}$. The term $4\left(F_0 - F\right)/T$ is simply the contribution from the conformal theory; the deviation from it is related to the conformal symmetry being broken by introducing the fundamental flavors and the external magnetic field. This breaking is manifest by non–vanishing $\tilde{c}$ and $\eta$ in equation (45) respectively. Recalling the relation between the energy density and the free energy density $E = F + TS$, and, using equation (45), we find that:

$$\begin{aligned} c_{V7} &= \left(\frac{\partial E}{\partial T}\right)_V \\ &= 3S_{D7} - 2\widetilde{\mathcal{N}}\pi^4\frac{\partial}{\partial T}(T^4\tilde{m}\tilde{c}) + 4\widetilde{\mathcal{N}}\pi^4\eta^2\frac{\partial}{\partial T}\left(T^4\frac{\partial\tilde{I}_{D7}}{\partial\eta^2}\right). \end{aligned} \tag{46}$$

Using the definition in equation (43), together with the above results and expanding up to first order in $\nu = N_f/N_c$, we get:

$$v^2 \approx \frac{1}{3}\left[1+\frac{\lambda N_f}{N_c}\frac{\pi^2}{6}\left(\tilde{m}\tilde{c}-\frac{1}{3}\tilde{m}^2\frac{\partial\tilde{c}}{\partial\tilde{m}}\right)-\frac{\lambda N_f}{N_c}\frac{\pi^2\eta^2}{3}\left(\frac{4}{3}\frac{\partial\tilde{I}_{D7}}{\partial\eta^2}+\frac{1}{3}\frac{\partial}{\partial\eta^2}(2\tilde{m}\tilde{c})\right)\right]+O(\nu^2). \tag{47}$$

The second and third term in equation (47) represent the deviation from the conformal value of 1/3 by the presence of the fundamental flavors and the external magnetic field. For convenience let us define $\delta v^2 = v^2 - 1/3$. It is possible to obtain an analytic expression for $\delta v^2$ in the limit of large bare quark mass and small magnetic field ($\tilde{m} \gg \sqrt{\eta}$). Using our previous analytic expressions, we get:

$$\delta v^2 \approx \lambda \frac{N_f}{N} \frac{\pi^2}{3} \left( \frac{2}{3}\eta^2 \log \tilde{m} - \frac{1}{6}\eta^2 \log\left(\frac{\eta^2}{4}\right) - \frac{1 - 24\tilde{m}^4\eta^2 + 8\eta^4}{72\tilde{m}^4} \right) + O\left(\frac{1}{\tilde{m}^5}\ .\right) \tag{48}$$

It is important to note that equation (48) is valid only up to first order in $\nu$. To proceed beyond the large bare quark mass and small magnetic field limit, we study numerically the velocity deviation, which is summarised in figure 11. We observe from figure 11(a) that, for small magnetic field, the deviation is similar to the zero magnetic field case; $\delta v^2$ approaches zero (corresponding to restoration of the conformal symmetry) from below in both the $T \to 0$ and $T \to \infty$ limits. However in presence of large magnetic field (see figure 11(d)), we see that $\delta v^2 > 0$, and the conformal value is never attained.

# 5 Meson Spectrum

In this section, we calculate the meson spectrum of the gauge theory. The mesons we are considering are formed from quark–antiquark pairs, so the relevant objects to consider are 7–7 strings. In our supergravity description, these strings are described by fluctuations (to second order in $\alpha'$) of the probe branes' action about the classical embeddings we found in the previous sections[22]. Studying the meson spectrum serves two purposes. First, tachyons in the meson spectrum from fluctuations of the classical embeddings indicate the instability of the embedding. Second, a massless meson satisfying a Gell-Mann-Oakes-Renner (GMOR) relation will confirm that spontaneous chiral symmetry breaking has occurred. As a reminder, in ref. [22], the exact meson spectrum for the $\mathrm{AdS}_5 \times S^5$ background was found to be given by:

$$M(n,\ell) \;=\; \frac{2m}{R^2}\sqrt{(n+\ell+1)(n+\ell+2)}\ , \tag{49}$$

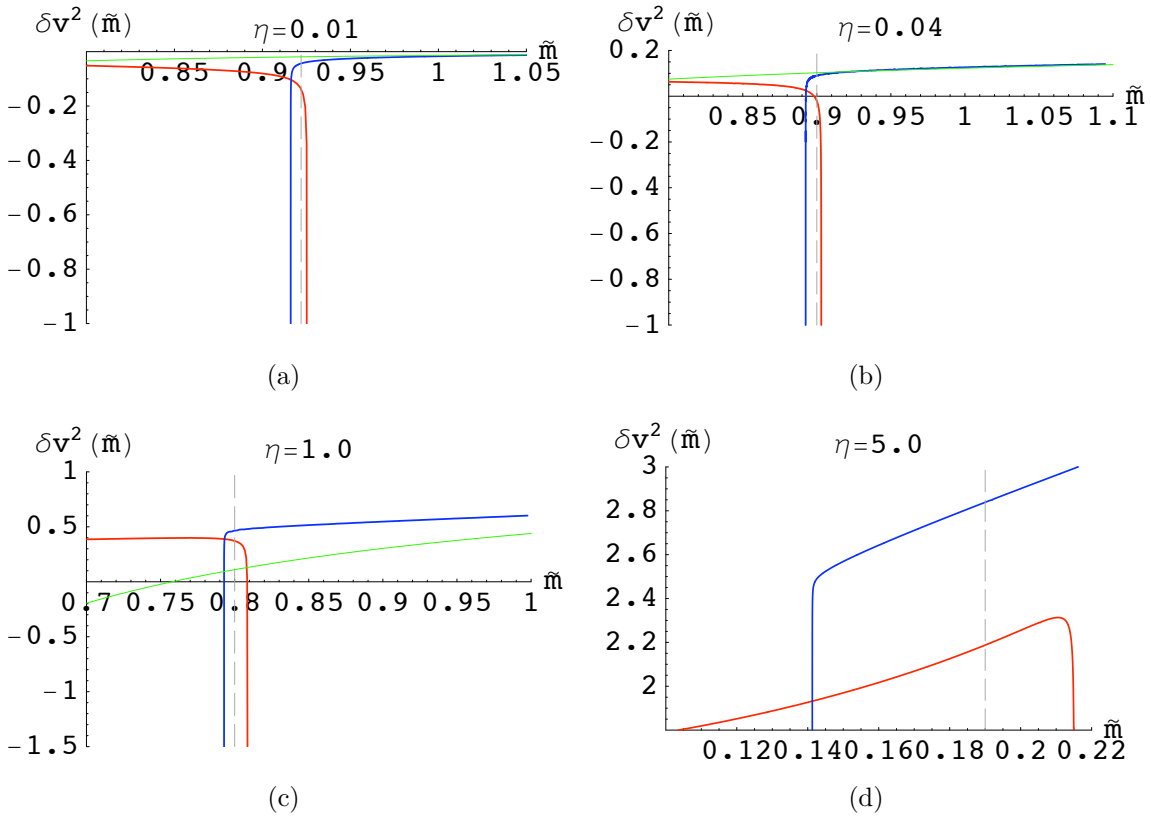


Figure 11: The deviation of the speed of sound from the conformal value in units of $(\nu\lambda)\pi^2/3$ in the presence of fundamental matter and an external magnetic field. The curves coming in from the left (red) correspond to black hole embeddings, and the curves coming in from the right (blue) correspond to Minkowski embeddings. The vertical dashed line represents the phase transition point, and the flatter dashed curves (green) correspond to the approximate analytic expression given in (48). We do not include the curve of the analytic result in 11(d) since the approximate formula is not valid for high magnetic fields.

where $\ell$ labels the order of the spherical harmonic expansion, and $n$ is a positive integer that represents the order of the mode. The relevant pieces of the action to second order in $\alpha'$ are:

$$\begin{aligned} S/N_f &= -T_{D7}\int d^8\xi\sqrt{g_{ab}+B_{ab}+2\pi\alpha' F_{ab}}+(2\pi\alpha')\,\mu_7\int_{\mathcal{M}_8} F_{(2)}\wedge B_{(2)}\wedge P\left[\tilde{C}_{(4)}\right] \\ &\quad +(2\pi\alpha')^2\,\mu_7\frac{1}{2}\int_{\mathcal{M}_8} F_{(2)}\wedge F_{(2)}\wedge P\left[C_{(4)}\right]\ , \end{aligned} \tag{50}$$

$$C_{(4)} = \frac{1}{g_s}\frac{u^4}{R^4}dt\wedge dx^1\wedge dx^2\wedge dx^3\ , \tag{51}$$

$$\tilde{C}_{(4)} = -\frac{R^4}{g_s}\left(1-\cos^4\theta\right)\sin\psi\cos\psi\ d\psi\wedge d\phi_2\wedge d\phi_3\wedge d\phi_1\ , \tag{52}$$

where $P\left[C_{(4)}\right]$ is the pull–back of the 4–form potential sourced by the stack of $N_c$ D3–branes, $P\left[\tilde{C}_{(4)}\right]$ is the pull–back of the 4–form magnetic dual to $C_{(4)}$, and $F_{(2)}$ is the Maxwell 2–form on the D7–brane worldvolume. At this point, we resort to a different set of coordinates than we have been using. Instead of using the coordinates $(\rho, L)$ introduced in equation (2), we return to the coordinates $(z = 1/u^2, \theta)$ because the analysis is simpler. We consider fluctuations of the form:

$$\theta = \theta_0(z) + 2\pi\alpha'\chi(\xi^a) \ , \tag{53}$$

$$\phi_1 = 2\pi\alpha'\Phi(\xi^a) \ , \tag{54}$$

where the indices $a, b = 0 \ldots 7$ run along the worldvolume of the D7–brane. $\theta_0(z)$ corresponds to the classical embedding from the classical equations of motion. Plugging the ansatz in equations (53) and (54) into the action and expanding to second order in $(2\pi\alpha')$, we get as second order terms in the lagrangian:

$$\begin{aligned}
-\mathcal{L}_{\chi^2} &= \frac{1}{2}\sqrt{-E}S^{ab}R^2\partial_a\chi\partial_b\chi - \frac{1}{2}\sqrt{-E}R^4\left(\theta_0'\right)^2 E^{zz}S^{ab}\partial_a\chi\partial_b\chi \\
&\quad + \frac{1}{2}\chi^2\left[\partial_\theta^2\sqrt{-E} - \partial_z\left(E^{zz}R^2\theta_0'\partial_\theta\sqrt{-E}\right)\right] \ , \\
-\mathcal{L}_{\Phi^2} &= \frac{1}{2}\sqrt{-E}S^{ab}R^2\sin^2\theta_0\partial_a\Phi\partial_b\Phi \ , \\
-\mathcal{L}_{F^2} &= \frac{1}{4}\sqrt{-E}S^{ab}S^{cd}F_{bc}F_{ad} \ , \\
-\mathcal{L}_{F-\chi} &= \chi F_{23}\left[\partial_z\left(\sqrt{-E}R^2\theta_0'E^{zz}J^{23}\right) - J^{23}\partial_\theta\sqrt{-E}\right] = \chi F_{23}f \ , \\
\mathcal{L}_{F^2}^{\mathrm{WZ}} &= \frac{1}{8}\frac{1}{z^2R^4}F_{mn}F_{op}\epsilon^{mnop} \ , \\
\mathcal{L}_{F-\Phi}^{\mathrm{WZ}} &= -\Phi F_{01}B_{23}R^4\sin\psi\cos\psi\partial_z\left(1-\cos^4\theta_0\right) = -\Phi F_{01}B_{23}R^4\sin\psi\cos\psi\partial_z K \ .
\end{aligned} \tag{55}$$

We have taken $E_{ab} = g_{ab}^{(0)} + B_{ab}$ to be the zeroth order contribution from the DBI action. In addition, we use that $E^{ab} = S^{ab} + J^{ab}$, where $S^{ab} = S^{ba}$ and $J^{ab} = -J^{ba}$. We use this notation for brevity. The indices $m, n, o, p = 4 \ldots 9$ run in the transverse directions to the D3–branes. From these lagrangian terms, we derive the equation of motion for $\chi$ to be:

$$\begin{aligned}
0 &= \partial_a\left(\sqrt{-E}S^{ab}R^2\left(\frac{1+4b^4z^4\left(\theta_0'\right)^2}{1+4z^2\left(\theta_0'\right)^2}\right)\partial_b\chi\right) - \chi\left[\partial_\theta^2\sqrt{-E} - \partial_z\left(E^{zz}R^2\theta_0'\partial_\theta\sqrt{-E}\right)\right] \\
&\quad - F_{23}\left[\partial_z\left(\sqrt{-E}R^2\theta_0'E^{zz}J^{23}\right) - J^{23}\partial_\theta\sqrt{-E}\right] \ .
\end{aligned} \tag{56}$$

The equation of motion for $\Phi$ is given by:

$$\partial_a\left(\sqrt{-E}S^{ab}R^2\sin^2\theta_0\partial_b\Phi\right) - F_{01}B_{23}R^4\sin\psi\cos\psi\partial_z K = 0 \ . \tag{57}$$

The equation of motion for $A_b$ is given by:

$$\partial_a \left( -\sqrt{-E} S^{aa'} S^{bb'} F_{a'b'} - \chi f \left( \delta^a_2 \delta^b_3 - \delta^a_3 \delta^b_2 \right) + B_{23} \Phi \partial_z K \left( \delta^a_0 \delta^b_1 - \delta^a_1 \delta^b_0 \right) \right.$$
$$\left. + \frac{1}{2} \frac{1}{z^2 R^4} \epsilon^{mnop} \delta^a_m \delta^b_n F_{op} \right) = 0 \, . \quad (58)$$

We are allowed to set $A_m = 0$ with the constraint (using that $S^{22} = S^{33}$):

$$S^{00} \partial_m \partial_0 A_0 + S^{11} \partial_m \partial_1 A_1 + S^{22} \partial_m \left( \partial_2 A_2 + \partial_3 A_3 \right) = 0$$

Therefore, we can consistently take $A_0 = \partial_1 A_1 = 0$, $\partial_2 A_2 = -\partial_3 A_3$. With this particular choice, we have as equations of motion for the gauge field:

$$\begin{aligned}
-\partial_0 \left( \sqrt{-E} S^{00} S^{11} \partial_0 A_1 \right) + \partial_z K B_{23} \partial_0 \Phi - \partial_z \left( \sqrt{-E} S^{zz} S^{11} \partial_z A_1 \right) & \\
- \partial_{\tilde{m}} \left( \sqrt{-E} S^{\tilde{m}\tilde{n}} S^{11} \partial_{\tilde{n}} A_1 \right) &= 0 \, , \\
-\partial_0 \left( \sqrt{-E} S^{00} S^{22} \partial_0 A_2 \right) + f \partial_3 \chi - \partial_z \left( \sqrt{-E} S^{zz} S^{22} \partial_z A_2 \right) & \\
- \partial_{\tilde{m}} \left( \sqrt{-E} S^{\tilde{m}\tilde{n}} S^{22} \partial_{\tilde{n}} A_2 \right) &= 0 \, , \\
-\partial_0 \left( \sqrt{-E} S^{00} S^{33} \partial_0 A_3 \right) - f \partial_2 \chi - \partial_z \left( \sqrt{-E} S^{zz} S^{33} \partial_z A_3 \right) & \\
- \partial_{\tilde{m}} \left( \sqrt{-E} S^{\tilde{m}\tilde{n}} S^{33} \partial_{\tilde{n}} A_3 \right) &= 0 \, ,
\end{aligned}$$

where the indices $\tilde{m}, \tilde{n}$ run over the $S^3$ that the D7–brane wraps. If we assume that $\partial_i \chi = 0$, we find that the equations for $A_2$ and $A_3$ decouple from $\chi$. Therefore, we can consistently take $F_{23} = 0$, or, in other words, $A_2 = A_3 = 0$. This simplifies the equations of motion that we need to consider to:

$$\begin{aligned}
0 &= \partial_a \left[ \sqrt{-E} S^{ab} R^2 \left( \frac{1 + 4 b^4 z^4 \left( \theta_0' \right)^2}{1 + 4 z^2 \left( \theta_0' \right)^2} \right) \partial_b \chi \right] - \chi \left[ \partial_\theta^2 \sqrt{-E} \right. \\
&\quad \left. - \partial_z \left( E^{zz} R^2 \theta_0' \partial_\theta \sqrt{-E} \right) \right] \, , \quad (59) \\
0 &= -\partial_0 \left( \sqrt{-E} S^{00} S^{11} \partial_0 A_1 \right) + \partial_z K B_{23} \partial_0 \Phi - \partial_z \left( \sqrt{-E} S^{zz} S^{11} \partial_z A_1 \right) \\
&\quad - \partial_{\tilde{m}} \left( \sqrt{-E} S^{\tilde{m}\tilde{n}} S^{11} \partial_{\tilde{n}} A_1 \right) \, , \quad (60) \\
0 &= \partial_a \left( \sqrt{-E} S^{ab} R^2 \sin^2 \theta_0 \partial_b \Phi \right) - F_{01} B_{23} R^4 \sin \psi \cos \psi \partial_z K \, . \quad (61)
\end{aligned}$$

In the proceeding sections, we will work out the solutions to these equations numerically using a shooting method. With an appropriate choice of initial conditions at the event horizon, which we explain below, we numerically solve these equations as an initial condition problem in Mathematica. Therefore, the D.E. solver routine "shoots" towards the boundary of the problem, and we extract the necessary data at the boundary.

## 5.1 The $\chi$ Meson Spectrum

In order to solve for the meson spectrum given by equation (59), we consider an ansatz for the field $\chi$ of the form:

$$\chi = h(\tilde{z}) \exp\left(-i\tilde{\omega}t\right) \ , \tag{62}$$

where we are using the same dimensionless coordinates as before, with the addition that:

$$z \ = \ b^{-2}\tilde{z} \quad , \quad \omega \ = \ R^{-2}b\,\tilde{\omega} \ .$$

In these coordinates, the event horizon is located at $\tilde{z} = 1$. Since there are two different types of embeddings, we analyze each case separately. We begin by considering black hole embeddings. In order to find the appropriate infrared initial conditions for the shooting method we use, we would like to understand the behavior of $h(\tilde{z})$ near the horizon. The equation of motion in the limit of $\tilde{z} \to 1$ reduces to:

$$h''(\tilde{z}) + \frac{1}{\tilde{z}-1}h'(\tilde{z}) + \frac{\tilde{\omega}^2}{16\left(\tilde{z}-1\right)^2}h(\tilde{z}) \ = \ 0 \ . \tag{63}$$

The equation has solutions of the form $(1-\tilde{z})^{\pm i\tilde{\omega}/4}$, exactly of the form of quasinormal modes [23]. Since the appropriate fluctuation modes are in–falling modes [24], we require only the solution of the form $(1-\tilde{z})^{-i\tilde{\omega}/4}$. This is our initial condition at the event horizon for our shooting method. In order to achieve this, we redefine our fields as follows:

$$h(\tilde{z}) \ = \ y(\tilde{z})(1-\tilde{z})^{-i\tilde{\omega}/4} \ ,$$

which then provides us with the following initial condition:

$$y(\tilde{z} \to 1) \ = \ \epsilon \ , \tag{64}$$

where $\epsilon$ is chosen to be vanishingly small in our numerical analysis. The boundary condition on $y'(\tilde{z} \to 1)$ is determined from requiring the equation of motion to be regular at the event horizon. The solution for the fluctuation field $y(\tilde{z})$ must be comprised of only a normalizable mode, which in turn determines the correct value for $\tilde{\omega}$. Since we are dealing with quasinormal modes for the black hole embeddings, $\tilde{\omega}$ will be complex; the real part of $\tilde{\omega}$ corresponds to the mass of the meson before it melts, and the imaginary part of $\tilde{\omega}$ is the inverse lifetime (to a factor of 2) [24]. We begin by considering the trivial embedding

$\theta_0(\tilde{z}) = 0$ (a black hole embedding). This embedding corresponds to having a zero bare quark mass. The equation of motion (59) simplifies tremendously in this case:

$$h''(\tilde{z}) + \left(\frac{2\tilde{z}}{\tilde{z}^2-1} - \frac{1}{\tilde{z}\left(1+\tilde{z}^2\eta^2\right)}\right) h'(\tilde{z}) + \frac{3+\tilde{z}\left(-3\tilde{z}+\tilde{\omega}^2\right)}{4\tilde{z}^2\left(\tilde{z}^2-1\right)^2} h(\tilde{z}) \;=\; 0\ . \tag{65}$$

We show solutions for $\tilde{\omega}$ in figure 12 as a function of the magnetic field $\eta$. In particular, we find the same additional mode discussed in ref. [25]. This mode becomes massless and eventually tachyonic at approximately $\eta \approx 9.24$. This point was originally presented in figure 8, where the intermediate unstable phase joins the trivial embedding. This is exactly when the $-\tilde{c}$ vs $\tilde{m}$ plot has negative slope for all black hole embeddings.

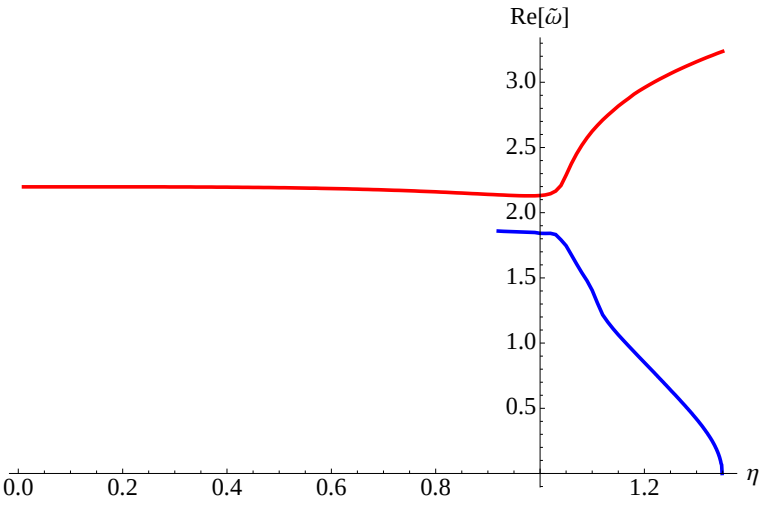


Figure 12: The $\chi$ meson mass as a function of magnetic field for the trivial embedding. The upper (red) curve is the generalization of the mode described in ref. [24]. The lower (blue) curve is the generalization the mode discussed in ref. [25]. We do not extend this second curve to small $\eta$ because the numerics become unreliable.

We now consider embeddings with non–zero bare quark mass. This means solving the full equation (59). We have both embeddings to consider; for the black hole embeddings, we will follow the same procedure presented above to solve for the complex $\tilde{\omega}$. We can still use the same procedure because in the limit of $\tilde{z} \to 1$, the equation of motion still reduces to equation (63). For the Minkowski embeddings, we do not have quasinormal modes, and $\tilde{\omega}$ is purely real. Therefore, we use as initial conditions:

$$\chi(\tilde{z} \to \tilde{z}_{\rm max}) \;=\; \epsilon\ , \tag{66}$$

$$\chi'(\tilde{z} \to \tilde{z}_{\rm max}) \;=\; \infty\ . \tag{67}$$

In figures 13 and 14, we show solutions for very different magnetic field values. In the former case, $\eta$ is small, and we do not have chiral symmetry breaking; in the latter, $\eta$ is large, and we have chiral symmetry breaking. It is important to note that in neither of the graphs do we find a massless mode at zero bare quark mass. In figure 13, we find that fluctuations about both the black hole and Minkowski embeddings become massless and tachyonic (we do not show this in the graph). The tachyonic phase corresponds exactly to the regions in the $-\tilde{c}$ vs $\tilde{m}$ plot with negative slope.

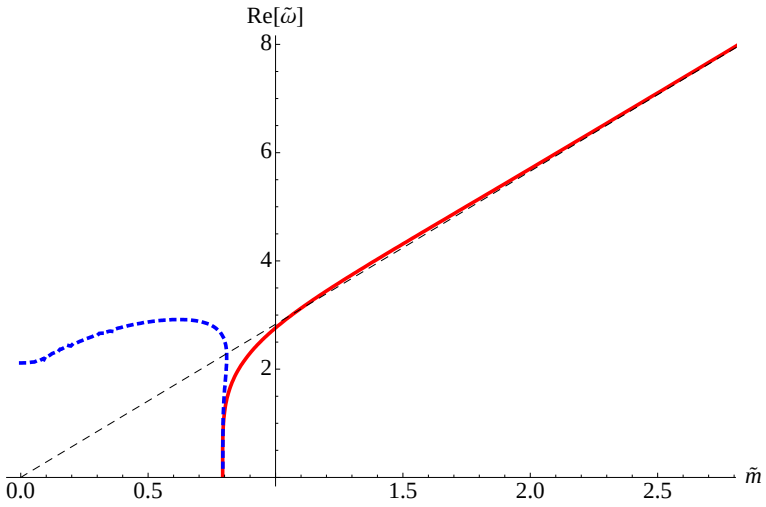


Figure 13: The $\chi$ meson mass as a function of bare quark mass for $\eta = 1$. The dashed (blue) curve corresponds to fluctuations about black hole embeddings. The solid (red) line corresponds to fluctuations about Minkowski emeddings. These modes have a purely real $\omega$. The straight dashed (black) line corresponds to the pure $AdS_5 \times S^5$ solution.

# 6 The $\Phi$ and $A$ Meson Spectra

Let us now consider the coupled fluctuations of $\Phi$ and $A$ in equations (60) and (61). We consider an ansatz (as before) of the form:

$$\begin{aligned} \Phi &= \phi(\tilde{z}) \exp(-i\tilde{\omega}t) \ , \\ A_1 &= A(\tilde{z}) \exp(-i\tilde{\omega}t) \ . \end{aligned}$$

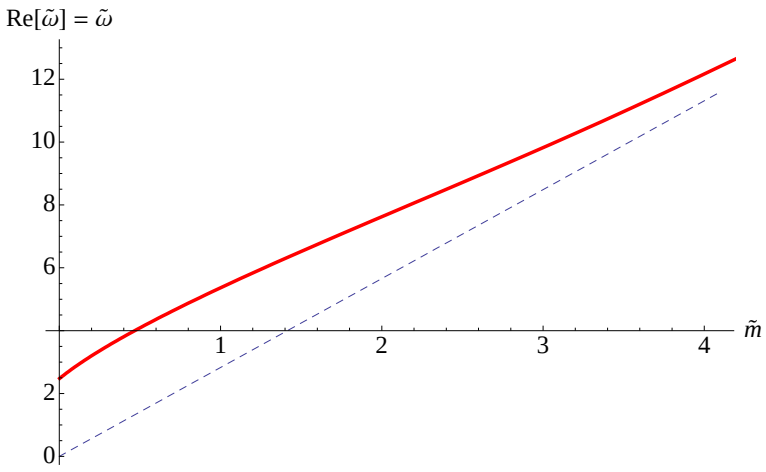


Figure 14: The $\chi$ meson mass as a function of bare quark mass for $\eta = 10$. The dashed (black) line corresponds to the pure $AdS_5 \times S^5$ solution.

It is interesting to note that, for the trivial embedding $\theta_0(\tilde{z}) = 0$, one of the coupled equations is equal to zero, and we simply have:

$$A''(\tilde{z}) + \frac{\tilde{z}\left(2+\eta^2\left(3\tilde{z}^2-1\right)\right)}{\left(\tilde{z}^2-1\right)\left(1+\tilde{z}^2\eta^2\right)}A'(\tilde{z}) + \frac{\tilde{\omega}^2}{4\tilde{z}\left(\tilde{z}^2-1\right)^2}A(\tilde{z}) \;=\; 0\ .$$

Again, we note that in the limit of $\tilde{z} \to 1$, we have:

$$A''(\tilde{z}) + \frac{1}{\tilde{z}-1}A'(\tilde{z}) + \frac{\tilde{\omega}^2}{16\left(\tilde{z}-1\right)^2}A(\tilde{z}) \;=\; 0\ .$$

This is exactly the form of equation (63), so $A(\tilde{z})$ has the same solutions of in–falling and outgoing solutions, which provides us with the necessary initial conditions for our shooting method. We show solutions for $\tilde{\omega}$ in figure 15. Unfortunately, we do not know how to solve for the quasinormal modes for other black hole embeddings. Since the equations of motion are coupled, we are unable to find an analytic solution for the fluctuations near the event horizon. This prevents us from using infrared initial conditions for our shooting method. However, we are actually more interested in searching for the "pion" of our system, which will occur when we have chiral symmetry breaking. In those cases, we are only dealing with Minkowski embeddings with a pure real $\omega$, so we may ignore the black hole embeddings. Since the equations of motion are coupled, it turns out that only for specific initial conditions will both fluctuations only be comprised of normalizable modes. We represent this by a

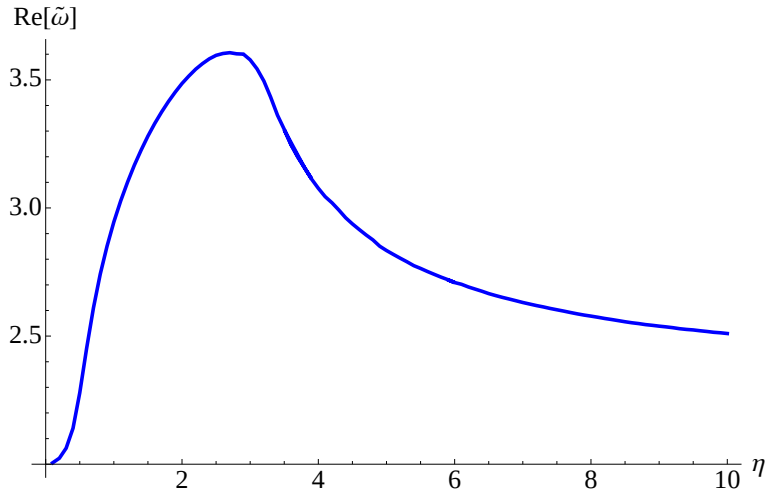


Figure 15: The $A$ meson mass as a function of magnetic field for the trivial embedding.

parameter $\alpha$ (which we must tune) as follows:

$$A(\tilde{z} \to \tilde{z}_{\rm max}) = i\cos\alpha \ , \tag{68}$$

$$\phi(\tilde{z} \to \tilde{z}_{\rm max}) = \sin\alpha \ . \tag{69}$$

The initial conditions on $A'$ and $\phi'$ are determined from the equations of motion. We show several solutions in figure 16. There are several important points to notice. First, we find that the lowest mode satisfies an GMOR relationship given by:

$$\tilde{\omega} \approx 1.1\tilde{m}^{1/2} \ . \tag{70}$$

Therefore, we have found the Goldstone boson of our system related to the breaking of chiral symmetry. Second, the modes exhibit the Zeemann splitting behavior that was discussed in ref. [15]. It is interesting that the various modes always cross each other at approximately $\tilde{m} \approx 2$. We have no intuitive explanation for this behavior.

# 7 Conclusions

We have extended the holographic study of large $N$ gauge theory in an external magnetic field, started in ref. [15], to the case of finite temperature, allowing us to study the properties of the quark dynamics when the theory is in the deconfined plasma phase.

The meson melting phase transition exists only below a critical value of the applied field. This is the critical value above which spontaneous chiral symmetry breaking is triggered

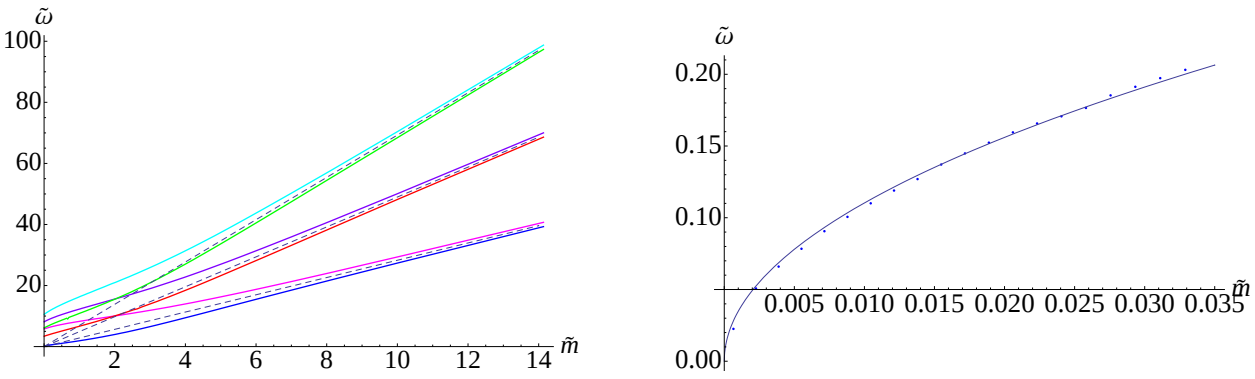


(a) Mass

(b) Zoom near zero bare quark mass for the lowest mode

Figure 16: Coupled $A-\phi$ fluctuations for $\eta = 10$. The dashed (black) line corresponds to the pure $AdS_5 \times S^5$ solution.

(in the case of zero mass). Above this value, regardless of the quark mass (or for fixed quark mass, regardless of the temperature) the system remains in a phase with a discrete spectrum of stable masses. Evidently, for these values of the field, it is magnetically favourable for the quarks and anti–quarks to bind together, reducing the degrees of freedom of the system , as can be seen from our computation of the entropy. Meanwhile, the magnetization and speed of sound are greater in this un–melted phase.

There have been non–perturbative studies of fermionic models in background magnetic field before, and there is a large literature (see *e.g.*, the reviews of refs. [27, 28], and the discussion of ref.[29] and references therein). Generally, those works use quite different methods to examine aspects of the physics — some primary non–perturbative tools are the Dyson–Schwinger equations in various truncations). Our results (and the zero temperature result obtained with these methods in the zero temperature case [15]) are consistent with the general expectations from those works, which is that strong magnetic fields are generically expected to be a catalyst for spontaneous chiral symmetry breaking in a wide class of models (see *e.g.*, refs. [30, 29, 27] for a discussion of the conjectured universality of this result).

While it is satisfying that our supergravity/string methods, which probe the gauge theory non–perturbatively *via* the holographic duality, confirm those other non–perturbative approaches, it would be interesting and potentially useful to compare the results in more detail, as this would (for example) allow a better understanding of the systematics of the Dyson–Schwinger truncation schemes. Whether or not such a direct comparison of these very different non–perturbative approaches is possible would also be interesting to study

in its own right, potentially shedding light on other non–perturbative phenomena in field theory that have been studied using such methods. This avenue of investigation is beyond the scope of this paper, however, and we leave it for future study.

## Acknowledgments

This work was supported by the US Department of Energy. This work was presented by cvj at the Newton Institute (Cambridge, UK) conference entitled: "Exploring QCD: Deconfinement, Extreme Environments, and Holography", 20–24 August 2007. We would like to thank the organizers for the opportunity to present and discuss our work and for a stimulating conference. We thank Nick Dorey and Nick Evans for drawing our attention to some of the literature on gauge theory in external magnetic fields.

# A Calculating the Physical Condensate

The condensate (density) is given by:

$$\langle\bar{\psi}\psi\rangle \;=\; \frac{\delta F}{\delta m_q}\;, \tag{71}$$

where $F$ is the free energy density and $m_q$ is the physical bare quark mass. The free energy density is given by equation (26), which we duplicate here:

$$\begin{aligned} F \;=\; & 2\pi^2 N_f T_{D7} b^4 \left[ \int_{\tilde{\rho}_{\rm min}}^{\tilde{\rho}_{\rm max}} d\tilde{\rho} \left( \tilde{\rho}^3 \left(1-\frac{1}{16\tilde{r}^8}\right)\left(1+\frac{16\eta^2\tilde{r}^4}{(4\tilde{r}^4+1)^2}\right)^{\frac{1}{2}} \sqrt{1+\tilde{L}'^2} - \tilde{\rho}^3 \right) \right. \\ & \left. -\frac{1}{4}\tilde{\rho}_{\rm min}^4 - \frac{1}{2}\eta^2 \log\tilde{\rho}_{\rm max} - \frac{1}{8}\eta^2(1+\log 4-\log\eta^2) \right]\;. \end{aligned}$$

Therefore, to calculate the condensate, we have:

$$\langle\bar{\psi}\psi\rangle \;=\; \frac{\delta F}{\delta m_q} = 2\pi\alpha' \frac{\delta F}{\delta m} = \frac{2\pi\alpha'}{b}\frac{\delta F}{\delta \tilde{m}} = \frac{2\pi\alpha'}{b}\frac{\delta F}{\delta \tilde{L}\left(\epsilon\right)}\;, \tag{72}$$

where we are using a new set of coordinates $\tilde{z} = 1/\tilde{\rho}$ such that $\epsilon = 1/\tilde{\rho}_{\rm max}$. In order to continue, we consider the variation of the free energy density:

$$\delta F \;=\; 2\pi^2 N_f T_{D7} b^4 \left[ \int_{\epsilon}^{\tilde{z}_{\rm max}} d\tilde{z} \left( \frac{\partial\tilde{\mathcal{L}}}{\partial\tilde{L}\left(\tilde{z}\right)} - \frac{d}{d\tilde{z}}\frac{\partial\tilde{\mathcal{L}}}{\partial\tilde{L}'\left(\tilde{z}\right)} \right)\delta\tilde{L}\left(\tilde{z}\right) + \frac{\partial\tilde{\mathcal{L}}}{\partial\tilde{L}'\left(\tilde{z}\right)}\delta\tilde{L}\left(\tilde{z}\right)\Big|_{\epsilon}^{\tilde{z}_{\rm max}} \right]\;. \tag{73}$$

The first term is set to zero by the equation of motion. The boundary term evaluated at $\tilde{z}_{\rm max}$ is zero since for Minkowski embeddings $L'(\tilde{z}_{\rm max}) = 0$ and for black hole embeddings $1 - 1/16\tilde{r}^8 = 0$. Therefore, we are left with:

$$\delta F \;=\; -2\pi^2 N_f T_{D7} b^4 \frac{\partial\tilde{\mathcal{L}}}{\partial\tilde{L}'\left(\tilde{z}\right)}\delta\tilde{L}\left(\epsilon\right)\Big|_{\tilde{z}\to\epsilon} = -4\pi^2 N_f T_{D7} b^4 \tilde{c}\delta\tilde{m}\;, \tag{74}$$

where we have used the asymptotic expansion of $\tilde{L}(\epsilon) = \tilde{m} + \tilde{c}z^2$. Therefore, our final expression for the condensate is given by:

$$\langle\bar{\psi}\psi\rangle \;=\; -8\pi^3\alpha' N_f T_{D7} b^3 \tilde{c} = -\frac{T^3\sqrt{\lambda}N_c N_f}{4}\tilde{c}\;. \tag{75}$$

# B The $\eta$ Variation

In calculating the magnetization, we need to consider the on–shell quantity:

$$\left(\frac{\delta\tilde{I}_{D7}}{\delta\eta}\right)_T ; \quad \tilde{I}_{D7} = \int d\tilde{\rho}\ \tilde{\mathcal{L}}(\tilde{\rho},\eta;\tilde{L},\tilde{L}') \ . \tag{76}$$

In our discussion, fixing the temperature is equivalent to fixing the bare quark mass. This is true because the two quantities $(T, m_q)$ are related inversely to each other by the dimensionless quantity $\tilde{m} = m/b = 2\pi\alpha' m_q/\pi R^2 T$. Therefore, we are interested in calculating:

$$\left(\frac{\delta\tilde{I}_{D7}}{\delta\eta}\right)_{\tilde{m}} = \int_{\tilde{\rho}_{\rm min}}^{\tilde{\rho}_{\rm max}} d\tilde{\rho}\left(\frac{\partial\tilde{\mathcal{L}}}{\partial\tilde{L}'}\frac{\delta\tilde{L}'}{\delta\eta} + \frac{\partial\tilde{\mathcal{L}}}{\partial\tilde{L}}\frac{\delta\tilde{L}}{\delta\eta} + \frac{\partial\tilde{\mathcal{L}}}{\partial\eta}\right) = \left(\frac{\partial\tilde{\mathcal{L}}}{\partial\tilde{L}'}\frac{\delta\tilde{L}}{\delta\eta}\right)_{\tilde{\rho}_{\rm min}}^{\tilde{\rho}_{\rm max}} + \int_{\tilde{\rho}_{\rm min}}^{\tilde{\rho}_{\rm max}} d\tilde{\rho}\frac{\partial\tilde{\mathcal{L}}}{\partial\eta} \ , \tag{77}$$

where we have used the equation of motion to simplify the expression. We can further simplify the expression by noting that the boundary term in equation (77) is zero, because

$$\frac{\partial\tilde{\mathcal{L}}}{\partial\tilde{L}'}\Big|_{\tilde{\rho}_{\rm min}} = 0 \ , \quad \text{and} \quad \frac{\partial\tilde{L}}{\partial\eta}\Big|_{\tilde{\rho}_{\rm max}} = \frac{\delta\tilde{m}}{\delta\eta} = 0 \ . \tag{78}$$

The last relation follows from the fact that we are taking the variational derivative with respect to $\eta$ at fixed $\tilde{m}$. Therefore, the necessary computation is simplified tremendously to:

$$\left(\frac{\delta\tilde{I}_{D7}}{\delta\eta}\right)_T = \left(\frac{\delta\tilde{I}_{D7}}{\delta\eta}\right)_{\tilde{m}} = \int_{\tilde{\rho}_{\rm min}}^{\tilde{\rho}_{\rm max}} d\tilde{\rho}\frac{\partial\tilde{\mathcal{L}}}{\partial\eta} \ . \tag{79}$$

# References


[1] L. Susskind and E. Witten, "The holographic bound in anti-de Sitter space," arXiv:hep-th/9805114.

[2] J. M. Maldacena, "The large N limit of superconformal field theories and supergravity," Adv. Theor. Math. Phys. **2**, 231 (1998) [Int. J. Theor. Phys. **38**, 1113 (1999)] [arXiv:hep-th/9711200].

[3] S. S. Gubser, I. R. Klebanov and A. M. Polyakov, Phys. Lett. B **428**, 105 (1998) [arXiv:hep-th/9802109].

[4] E. Witten, Adv. Theor. Math. Phys. **2**, 253 (1998) [arXiv:hep-th/9802150].

[5] E. Witten, Adv. Theor. Math. Phys. **2**, 505 (1998) [arXiv:hep-th/9803131].

[6] A. Karch and E. Katz, "Adding flavor to AdS/CFT," *JHEP* **06** (2002) 043, `hep-th/0205236`.

[7] J. Babington, J. Erdmenger, N. J. Evans, Z. Guralnik, and I. Kirsch, "Chiral symmetry breaking and pions in non-supersymmetric gauge / gravity duals," *Phys. Rev.* **D69** (2004) 066007, `hep-th/0306018`.

[8] M. Kruczenski, D. Mateos, R. C. Myers, and D. J. Winters, "Towards a holographic dual of large-N(c) QCD," *JHEP* **05** (2004) 041, `hep-th/0311270`.

[9] E. Shuryak, "Why does the quark gluon plasma at RHIC behave as a nearly ideal fluid?," Prog. Part. Nucl. Phys. **53**, 273 (2004) [arXiv:hep-ph/0312227].

[10] G. Policastro, D. T. Son and A. O. Starinets, "The shear viscosity of strongly coupled N = 4 supersymmetric Yang-Mills Phys. Rev. Lett. **87**, 081601 (2001) [arXiv:hep-th/0104066].

[11] P. Kovtun, D. T. Son and A. O. Starinets, "Holography and hydrodynamics: Diffusion on stretched horizons," JHEP **0310**, 064 (2003) [arXiv:hep-th/0309213].

[12] A. Buchel and J. T. Liu, "Universality of the shear viscosity in supergravity," Phys. Rev. Lett. **93**, 090602 (2004) [arXiv:hep-th/0311175].

[13] H. Liu, K. Rajagopal and U. A. Wiedemann, "Calculating the jet quenching parameter from AdS/CFT," Phys. Rev. Lett. **97**, 182301 (2006) [arXiv:hep-ph/0605178].

[14] S. S. Gubser, "Drag force in AdS/CFT," Phys. Rev. D **74**, 126005 (2006) [arXiv:hep-th/0605182].

[15] V. G. Filev, C. V. Johnson, R. C. Rashkov, and K. S. Viswanathan, "Flavoured large N gauge theory in an external magnetic field," `hep-th/0701001`.

[16] D. Mateos, R. C. Myers, and R. M. Thomson, "Holographic Phase Transitions with Fundamental Matter," `hep-th/0605046`.

[17] T. Albash, V. Filev, C. V. Johnson, and A. Kundu, "A Topology-Changing Phase Transition and the Dynamics of Flavour," `hep-th/0605088`.

[18] T. Albash, V. Filev, C. V. Johnson, and A. Kundu, "Global currents, phase transitions, and chiral symmetry breaking in large N(c) gauge theory," hep-th/0605175.

[19] D. Mateos, R. C. Myers, and R. M. Thomson, "Thermodynamics of the brane," hep-th/0701132.

[20] V. Balasubramanian and P. Kraus, "A stress tensor for anti-de Sitter gravity," Commun. Math. Phys. **208**, 413 (1999) [arXiv:hep-th/9902121].

[21] A. Karch, A. O'Bannon, and K. Skenderis, "Holographic renormalization of probe D-branes in AdS/CFT," *JHEP* **04** (2006) 015, hep-th/0512125.

[22] M. Kruczenski, D. Mateos, R. C. Myers, and D. J. Winters, "Meson spectroscopy in AdS/CFT with flavour," *JHEP* **07** (2003) 049, hep-th/0304032.

[23] A. O. Starinets, "Quasinormal modes of near extremal black branes," *Phys. Rev.* **D66** (2002) 124013, hep-th/0207133.

[24] C. Hoyos, K. Landsteiner, and S. Montero, "Holographic meson melting," hep-th/0612169.

[25] V. G. Filev, "Criticality, Scaling and Chiral Symmetry Breaking in External Magnetic Field," arXiv:0706.3811 [hep-th].

[26] J. Erdmenger, R. Meyer, and J. Shock, to appear.

[27] V. A. Miransky, "Dynamics of QCD in a strong magnetic field," arXiv:hep-ph/0208180.

[28] S. Y. Wang, "Progress on chiral symmetry breaking in a strong magnetic field," arXiv:hep-ph/0702010.

[29] G. W. Semenoff, I. A. Shovkovy and L. C. R. Wijewardhana, "Universality and the magnetic catalysis of chiral symmetry breaking," Phys. Rev. D **60**, 105024 (1999) [arXiv:hep-th/9905116].

[30] V. P. Gusynin, V. A. Miransky and I. A. Shovkovy, "Dimensional reduction and catalysis of dynamical symmetry breaking by a Nucl. Phys. B **462**, 249 (1996) [arXiv:hep-ph/9509320].